University of Montana

ScholarWorks at University of Montana

Numerical Terradynamic Simulation Group Publications

Numerical Terradynamic Simulation Group

6-2014

Surface water inundation in the boreal- Arctic: potential impacts on regional methane emissions

Jennifer D. Watts
University of Montana - Missoula

John S. Kimball
University of Montana - Missoula

Annett Bartsch
University of Salzburg

Kyle C. McDonald
City College of New York

Follow this and additional works at: https://scholarworks.umt.edu/ntsg_pubs

Let us know how access to this document benefits you.

Recommended Citation

Surface water inundation in the boreal-Arctic: potential impacts on regional methane emissions

Jennifer D Watts[1,2], John S Kimball[1,2], Annett Bartsch[3,4,5,6] and Kyle C McDonald[7]

[1] Flathead Lake Biological Station, The University of Montana, 32125 Bio Station Lane, Polson, MT 59860, USA
[2] Numerical Terradynamic Simulation Group, CHCB 428, 32 Campus Drive, The University of Montana, Missoula, MT 59812, USA
[3] Austrian Polar Research Institute, c/o Universität Wien, Althanstraße 14, A-1090 Vienna, Austria
[4] Department of Geodesy and Geoinformation, Vienna University of Technology, Gusshausstrasse 27-29, A-1040 Vienna, Austria
[5] Department of Geography, Ludwig Maximilians University, Luisenstrasse 37, D-80333 Munich, Germany
[6] Department of Geoinformatics and Z_GIS, University of Salzburg, Hellbrunnerstr. 37, A-5020 Salzburg, Austria
[7] Department of Earth and Atmospheric Sciences, The City College of New York, New York, NY 10031, USA

E-mail: jennifer.watts@ntsg.umt.edu

Abstract

Northern wetlands may be vulnerable to increased carbon losses from methane (CH_4), a potent greenhouse gas, under current warming trends. However, the dynamic nature of open water inundation and wetting/drying patterns may constrain regional emissions, offsetting the potential magnitude of methane release. Here we conduct a satellite data driven model investigation of the combined effects of surface warming and moisture variability on high northern latitude ($\geqslant 45° N$) wetland CH_4 emissions, by considering (1) sub-grid scale changes in fractional water inundation (Fw) at 15 day, monthly and annual intervals using 25 km resolution satellite microwave retrievals, and (2) the impact of recent (2003–11) wetting/drying on northern CH_4 emissions. The model simulations indicate mean summer contributions of 53 Tg CH_4 yr^{-1} from boreal-Arctic wetlands. Approximately 10% and 16% of the emissions originate from open water and landscapes with emergent vegetation, as determined from respective 15 day Fw means or maximums, and significant increases in regional CH_4 efflux were observed when incorporating satellite observed inundated land fractions into the model simulations at monthly or annual time scales. The satellite Fw record reveals widespread wetting across the Arctic continuous permafrost zone, contrasting with surface drying in boreal Canada, Alaska and western Eurasia. Arctic wetting and summer warming increased wetland emissions by 0.56 Tg CH_4 yr^{-1} compared to the 2003–11 mean, but this was mainly offset by decreasing emissions (-0.38 Tg CH_4 yr^{-1}) in sub-Arctic areas experiencing surface drying or cooling. These findings underscore the importance of monitoring changes in surface moisture and temperature when assessing the vulnerability of boreal-Arctic wetlands to enhanced greenhouse gas emissions under a shifting climate.

1. Introduction

Wetlands and lakes cover approximately 2–8% of the boreal-Arctic region (Watts *et al* 2012), with large fluctuations in surface water extent resulting from seasonal melt cycles, summer precipitation and drought events (Schroeder *et al* 2010, Bartsch *et al* 2012, Helbig *et al* 2013). Wet surface conditions and characteristically colder temperatures greatly reduce the rate of organic carbon decomposition in northern wetland environments (Harden *et al* 2012, Elberling *et al* 2013). As a result, over 50% of the global soil organic carbon pool is stored in these regions (Turetsky *et al* 2007, Hugelius *et al* 2013). Landscapes with inundated or moist surfaces are particularly vulnerable to carbon loss as methane (CH_4) (Turetsky *et al* 2008, Fisher *et al* 2011, Olefeldt *et al* 2013). Contemporary estimates of methane source contributions from northern wetlands range between 12 and 157 Tg CH_4 yr^{-1} (Petrescu *et al* 2010, McGuire *et al* 2012, Meng *et al* 2012, Gao *et al* 2013), and may double over the next century if surface temperatures continue to rise (Koven *et al* 2011, Schneider von Deimling *et al* 2012).

Various wetland maps have been used to define the extent of methane emitting area (Matthews and Fung 1987, Aselmann and Crutzen 1989, Reeburgh *et al* 1998, Lehner and Döll 2004, Schneider *et al* 2009, Glagolev *et al* 2011), but their static nature fails to capture dynamic spatiotemporal variations in surface wetness within boreal-Arctic environments. As a result, modeling studies are increasingly using satellite based inundation data to characterize the impact of changing surface water coverage on regional methane emissions (Petrescu *et al* 2010, Riley *et al* 2011, Zhu *et al* 2011, Meng *et al* 2012, Bohn *et al* 2013, Wania *et al* 2013). These datasets include the GIEMS (Global Inundation Extent from Multi-Satellites) record (Prigent *et al* 2007, Papa *et al* 2010) that estimates monthly inundation within 0.25° resolution grid cells using microwave observations from the Special Sensor Microwave/Imager (SSM/I) and the ERS scatterometer. However, the GIEMS record only spans from 1993 to 2007 and relies on visible (0.58–0.68 μm) and near-infrared (0.73–1.1 μm) Advanced Very High Resolution Radiometer (AVHRR) data to account for vegetation canopy effects on microwave retrievals (Papa *et al* 2010). An alternative method, described by Schroeder *et al* (2010) and integrated into methane studies for western Siberia (Bohn *et al* 2013, Wania *et al* 2013), avoids the use of optical/infrared sensor information by incorporating QuikSCAT scatterometer and 6.9 GHz passive microwave data from the Advanced Microwave Scanning Radiometer for EOS (AMSR-E) to determine 25 km grid fractional water coverage at 10 day intervals.

A recent approach introduced by Jones *et al* (2010) uses AMSR-E 18.7 and 23.8 GHz, H- and V- polarized brightness temperatures to retrieve 25 km resolution daily fractional open water (Fw) inundation, and does not require ancillary information (e.g. AVHRR optical or QuikSCAT radar) to account for microwave scattering effects from intervening atmosphere and vegetation. The Jones *et al* (2010) AMSR-E Fw data have been used to evaluate recent seasonal and inter-annual inundation variability across the northern high latitudes and permafrost regions, with a demonstrated sensitivity to changes in the surface water balance, and a relatively low observation spatial uncertainty of approximately 4% (Watts *et al* 2012). The higher frequency 18.7 and 23.8 GHz brightness temperatures used to derive the AMSR-E Fw retrievals also minimize signal sensitivity to underlying soil moisture conditions (Jones *et al* 2010, Watts *et al* 2012). Although satellite optical and radar remote sensing can characterize wetland and open water distributions at finer (⩽150 m resolution) scales (Bartsch *et al* 2012, Rover *et al* 2012, Bohn *et al* 2013, Muster *et al* 2013), this information is often constrained to localized analyses with minimal repeat observations and is not yet conducive for the pan-Arctic wide monitoring of surface inundation.

This study examines the potential implications of recent (2003–11) variability in surface wetness on methane efflux from northern high latitude (⩾45° N) wetlands, and the contrasting influence of regional changes in moisture and temperature on summer (May through September) emission budgets using satellite remote sensing and reanalysis information. We postulate that seasonal and inter-annual fluctuations in surface inundation can greatly limit the magnitude of methane release from wetland environments, particularly if summer warming coincides with periods of drought. Conversely, northern wetlands may be more susceptible to methane emissions when the extent and duration of surface wetness is sustained or increasing. We conducted a series of carbon and climate sensitivity simulations using the Joint UK Land Environment Simulator (JULES) methane emissions model (Clark *et al* 2011, Bartsch *et al* 2012), with input Fw means and maximums at 15 day, monthly, and annual intervals as derived from an AMSR-E global daily land parameter record (Jones *et al* 2010, Jones and Kimball 2011a). In this study, Fw is defined as the proportional surface water cover within 25 km equal area AMSR-E grid cells (Watts *et al* 2012), and includes inundated soils, open water (e.g. lake bodies) and landscapes with emergent vegetation. We then evaluated the impact of recent temperature variability and wetting/drying on methane emission budgets for the northern wetland regions.
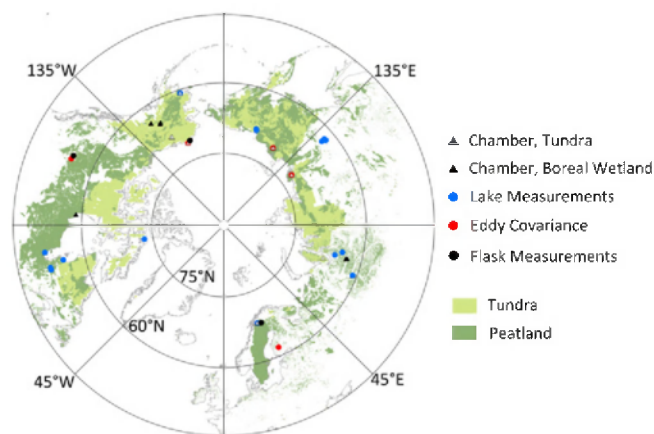
Figure 1. Locations of tower eddy covariance, flux chamber, lake and flask measurement sites used to verify methane emission simulations for the boreal-Arctic ($\geqslant 45°$ N) peatland (based on data provided by Gunnarsson and Löfroth 2009, Yu *et al* 2010, Franzén *et al* 2012) and RECCAP tundra domain.

2. Methods

2.1. Study region

The land area considered in this analysis was determined using boreal-Arctic peatland maps (i.e. Gunnarsson and Löfroth 2009, Yu *et al* 2010, Franzén *et al* 2012), and the Regional Carbon Cycle and Assessment Processes (REC-CAP) tundra domain (McGuire *et al* 2012). To coincide with the spatial extent of AMSR-E Fw coverage, we removed grid cells having $\geqslant 50\%$ permanent ice or open water cover using the UMD Moderate Resolution Imaging Spectroradiometer (MODIS) land cover product (described in Jones *et al* 2010), and applied a conservative 25 km coastline buffer to minimize Fw retrieval contamination by ocean water. The resulting study region spans approximately 1.6×10^{7} km^2 (figure 1), and contains 70% of northern continuous and discontinuous permafrost affected landscapes (Brown *et al* 1998).

2.2. Model description and calibration

The JULES model approach (Clark *et al* 2011, Bartsch *et al* 2012) accounts for the major factors (i.e. temperature, carbon substrate availability, landscape wetness) that control global methane emissions (Bloom *et al* 2010, Olefeldt *et al* 2013). Albeit relatively simple and lacking in detailed physical processes, this method is useful for pan-Arctic simulations because it avoids extensive parameterization requirements that can substantially increase estimate uncertainty (Riley *et al* 2011). The model regulates methane emissions according to available carbon substrate (C, kg m^{-2}) and an efflux rate constant (k_{CH_4}, d^{-1}) that is modified by a temperature dependent Q_{10} factor (Gedney *et al* 2004, Clark *et al* 2011). The temperature effects on methane production are controlled using daily input Modern Era Retrospective-analysis for Research and Applications (MERRA) surface soil temperature (T_s, in kelvin) and a thermal reference state (T_0,

273.15 K):

$$F_{CH_4} = C \times k_{CH_4} \times Q_{10}^{(T_s - T_0)/10} \times FThw. \tag{1}$$

For this analysis, we limit our investigation to non-frozen surface conditions defined using daily satellite passive microwave sensor derived binary (0 or 1) freeze/thaw (*FThw*) constraints (Kim *et al* 2013). The resulting daily fluxes (F_{CH_4}, CH$_4$ m^{-2}) were averaged over a 15 day time step and scaled to the 25 km grid cell domain (tonne CH$_4$ cell^{-1}) using Fw and volumetric soil moisture (θ, m^3/m^3) information to regulate landscape methane emissions. Methane efflux from inundated portions of the grid-cell were assumed to be non-inhibited, whereas non-inundated cell fractions ($1 - Fw$) were weighted by θ to account for reduced methane loss due to oxidation. In this study, the emissions weighting process was applied at a 15 day time step to address potential delays in methanogen response following surface wetting or drying (Blodau and Moore 2003, Turetsky *et al* 2014).

The daily input T_s and θ ($\leqslant 10$ cm soil depth) records were obtained from the NASA GEOS-5 MERRA Land reanalysis archive with native $0.5° \times 0.6°$ resolution (Reichle *et al* 2011) and posted to a 25 km resolution polar equal-area scalable earth grid consistent with the AMSR-E Fw data. The MERRA land parameters have been evaluated for high latitude regions, with favorable correspondence in relation to independent satellite microwave and *in situ* observations (Yi *et al* 2011, Watts *et al* 2014). Soil metabolic carbon (C$_{met}$) pools obtained from a Terrestrial Carbon Flux (TCF) model (Kimball *et al* 2009, Yi *et al* 2013) were used as the substrate for methanogenesis. The TCF carbon estimates reflect daily changes in labile plant residues and root exudates, and have been evaluated against existing soil organic carbon inventory records for the high latitude regions (described in Yi *et al* 2013). The C$_{met}$ inputs (kg C m^{-2} d^{-1}) were generated for the study region by a 1000 yr spin-up of the model using a 10 yr (2000–09) record of MODIS 1 km resolution Normalized Difference Vegetation Index, MERRA daily surface meteorology and soil moisture inputs.

The JULES model k_{CH_4} and Q_{10} parameters were calibrated using mean monthly eddy covariance methane fluxes (mg CH$_4$ m^{-1} d^{-1}) from five northern wetland tower sites (figure 1) that are described in the published literature (i.e. Rinne *et al* 2007, Sachs *et al* 2008, Wille *et al* 2008, Zona *et al* 2009, Long *et al* 2010, Parmentier *et al* 2011), in conjunction with mean MERRA reanalysis C$_{met}$ and T_s climatology over the 2003–11 summer (May through September) period. A resulting Q_{10} value of 3.7 and a k_{CH_4} rate of 3.7×10^{-5} d^{-1} minimized the root mean square error (RMSE) differences between the model and flux tower observations at 17.62 mg CH$_4$ m^{-2} d^{-1}. A Q_{10} of 3.7 was also used by Clark *et al* (2011) and is similar to those reported in other studies (Ringeval *et al* 2010, Waldrop *et al* 2010, Lupascu *et al* 2012). Further model verification was also obtained by evaluating summer flux chamber measurements (see supplementary table S1) from tundra ($n = 15$ site records), boreal wetland ($n = 11$) and lake ($n = 17$) locations.

2.3. Regional simulations

Grid-scale (25 km) wetland methane emissions were obtained using dynamic 15 day, monthly and annual summer AMSR-E Fw means or maximums from 2003 to 2011, to examine the potential impact of temporal Fw scaling on methane emission estimates. Methane simulations were also examined using a static mean summer Fw map derived from the 2003–11 record. The regional simulations were evaluated against NOAA ESRL atmospheric methane flask measurements (Dlugokencky *et al* 2013) from Barrow, AK, Lac LaBiche, CN, and Pallas Sammaltunturi, FI, to assess the ability of the model to capture between-year changes in methane concentrations that may correspond with fluctuations in wetland methane emissions (Lelieveld *et al* 1998). For Barrow and Sammaltunturi, the dry air mole fractions were available from 2003 through 2011; the Lac LaBiche data were available from 2008 onward. A Hybrid Single Particle Lagrangian Integrated Trajectory (HYSPLIT; Draxler and Rolph 2013, Rolph 2013) model, with a 100 m receptor point altitude and input GDAS-1 meteorology (Rodell *et al* 2004), was used to obtain backward (30 day) atmospheric trajectories for each flask site, and showed the dominant source contributions at Barrow to originate primarily from northern Alaska, the Yukon River basin eastward to the Northwest Territories, and eastern Siberia. For the respective Lac LaBiche and Sammaltunturi locations, the major source regions were from northern Canada, or extending from Scandinavia eastward into western Russia. To determine the relative correspondence between modeled annual methane emission contributions and observed mean summer dry air mole fractions, Pearson product-moment correlation coefficients (r) were derived using spatial means from a 3×3 grid cell window centered on each flask location. Regional point correlation maps (Ding and Wang 2005) were also obtained by evaluating r (e_j, a_k) for each grid cell within the methane source regions, where e_j is the modeled mean summer emissions time series at a given cell location and a_k is the atmospheric methane concentration time series at a flask sampling site.

Regional changes in surface water coverage, soil moisture and temperature were evaluated using a non-parametric Mann-Kendall trend analysis that accounts for serial correlation prior to determining trend significance (Yue *et al* 2002, Watts *et al* 2012). The Kendall rank correlations were applied to the mean summer AMSR-E Fw, and MERRA T_s and θ records on a per-grid cell basis from 2003 to 2011. Trend significance was determined at a minimum 95% ($p < 0.05$) probability level. The Kendall trend was also applied to the modeled cumulative annual methane emissions to identify regions that may be vulnerable to increasing anaerobic carbon losses. A linear regression analysis was then used to determine the rate of change in the annual emission estimates.

3. Results and discussion

3.1. Model evaluation against in situ methane flux observations

The model simulations captured overall temporal variability ($r^2 = 0.65$, $p < 0.05$) observed in the monthly tower eddy covariance records, with a RMSE value of $17.6 \, \text{mg CH}_4 \, \text{m}^{-2} \, \text{d}^{-1}$ that is similar to other regional studies (Meng *et al* 2012, Zhu *et al* 2013). Significant differences ($\alpha = 0.05$; two-sample t-test with unequal variance) were not observed (figure S1) between the model estimates and mean monthly tower eddy covariance ($t = 1.45$, $p = 0.15$), boreal chamber ($t = 0.05$, $p = 0.96$), and northern lake ($t = 0.79$, $p = 0.45$) fluxes. However, the modeled fluxes were significantly smaller ($t = 3.67$, $p < 0.01$) than the tundra chamber observations and did not adequately capture larger ($>140 \, \text{mg CH}_4 \, \text{m}^{-2} \, \text{d}^{-1}$) eddy covariance fluxes from a peatland site in northern Sweden (Jackowicz-Korczyński *et al* 2010). These discrepancies may reflect the presence of tall sedges (e.g. *E. angustifolium*), which can substantially increase emission rates through aerenchymateous tissue pathways (Joabsson *et al* 1999), or the limited representation of landscape scale emissions by chamber measurements given the potentially large contrasts in methane fluxes from dry and wet vegetation communities (Parmentier *et al* 2011) and functional groups (Kao-Kniffin *et al* 2010). The modeled methane fluxes were within the 5–140 $\text{mg CH}_4 \, \text{m}^{-2} \, \text{d}^{-1}$ range observed in the lake measurements (Zimov *et al* 1997, Laurion *et al* 2010, Desyatkin *et al* 2009, Sabrekov *et al* 2012), although these observations primarily reflect diffusive gas release and background bubbling instead of episodic ebullition events. As a result, the model simulations may underestimate ebullition release from open water bodies, particularly in carbon-rich thermokarst regions characterized by methane seeps (Walter *et al* 2006). However, the fraction of lake bodies exhibiting this seep behavior is not well quantified, and a recent analysis of sub-Arctic lakes reported that summer ebullition events averaged only $13 \, \text{mg CH}_4 \, \text{m}^{-2} \, \text{d}^{-1}$, with a low probability of bubble fluxes exceeding $200 \, \text{mg m}^{-2} \, \text{d}^{-1}$ (Wik *et al* 2013).

3.2. Regulatory effects of surface water and temperature on regional methane emissions

3.2.1. Wetland inundation characteristics. Approximately 5% ($8.4 \times 10^5 \, \text{km}^2 \pm 6\%$ SE) of the boreal-Arctic domain was inundated with surface water during the non-frozen summer season, as indicated by the 2003–11 AMSR-E Fw retrieval means. Over 63% of the wetlands were located in North America, primarily within the Canadian Shield region, and the majority of inundation occurred above 59° N within major wetland complexes, including the Ob-Yenisei and Kolyma Lowlands in Siberia (figure 2). A strong seasonal pattern in surface water was observed across the high latitudes, with an abrupt increase in May or early June following surface ice and snow melt, and the onset of spring precipitation (figure 3). In Eurasia, peak inundation occurred in June, followed by a gradual decline with summer drought
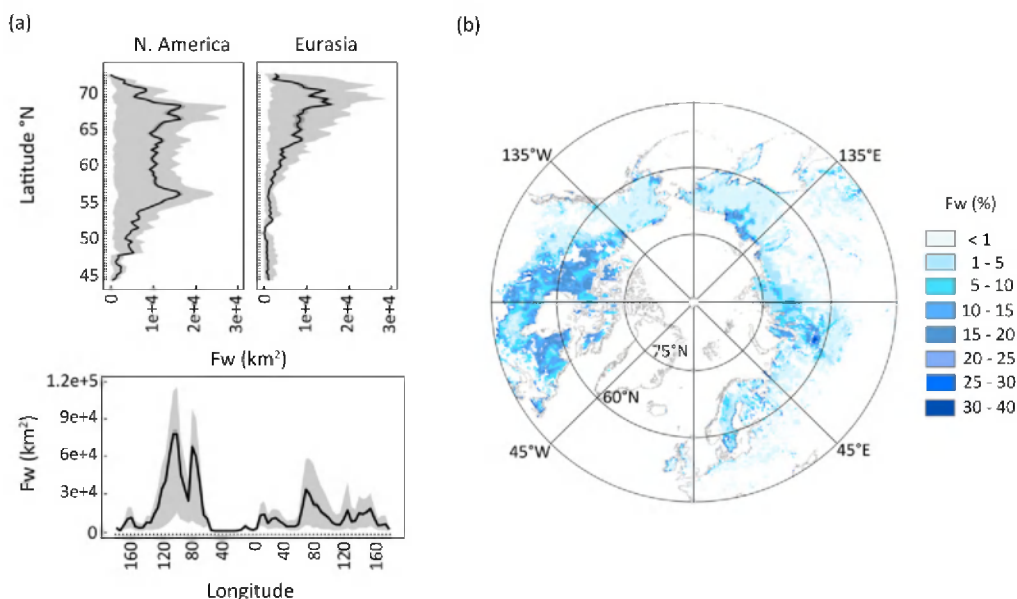
Figure 2. Regional variability in fractional surface water (Fw) within the northern ($\geqslant 45°$ N) wetland regions by (a) latitudinal and longitudinal distribution and (b) pan-Arctic domain; black lines and dark gray shading in (a) denote respective Fw spatial means and the associated 95% CI. Light gray shading indicates corresponding Fw minima and maxima. A multi-year (2003–11) mean of daily summer AMSR-E Fw retrievals was used to derive the spatial extent of inundation.
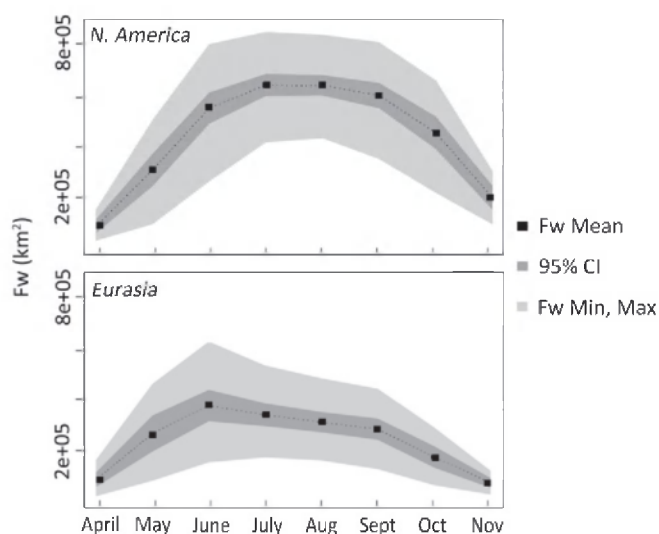

Figure 3. Seasonal (2003–11) variability in AMSR-E Fw inundation (km^2) within the boreal-Arctic wetland domain. The mean monthly Fw climatology is indicated in black, and corresponding 95% CI (Fw minima, maxima) are denoted by dark (light) gray shading.

and increased evaporative demand (Rawlins *et al* 2009, Schroeder *et al* 2010, Bartsch *et al* 2012, Watts *et al* 2012). In North America, the seasonal expansion of surface water continued through July, before beginning to subside with the onset of surface freezing.

The influence of wet/dry cycles on surface water extent was evident throughout the boreal-Arctic region. The summer of 2004 was the driest observed over the AMSR-E Fw record, with a 6% decrease in inundation from the long-term mean

that coincided with drought conditions across the Arctic Basin and Alaska (Rinsland *et al* 2007, Zhang *et al* 2008, Jones *et al* 2013). Summer 2008 was the wettest in North America, with a 3% increase in Fw coverage that was also reflected in positive drainage anomalies observed in the Mackenzie River basin (Watts *et al* 2012). The wettest summer in Eurasia occurred in 2007, particularly within the Ob, Lena and Kolyma drainage basins, with a 7% increase in surface water that coincided with regionally high summer temperatures (Dlugokencky *et al* 2009), snow melt and summer precipitation, and record river discharge (Rawlins *et al* 2009, Zhang *et al* 2013).

3.2.2. Regional summer methane simulations. Summer methane emissions estimated for non-inundated land fractions averaged 47.8 ± 1.8 Tg CH_4 yr^{-1} over the northern wetlands. This increased to 53.2 ± 1.9 Tg CH_4 yr^{-1} when also considering contributions from inundated landscapes based on the 15 day AMSR-E Fw means. These results are within the range of emissions (39 to 89 Tg CH_4 yr^{-1}) reported from previous modeling studies using other satellite-based Fw retrievals (table 1; Petrescu *et al* 2010, Ringeval *et al* 2010, Riley *et al* 2011, Spahni *et al* 2011, Wania *et al* 2013), but are higher than those from atmospheric inversion analyses of northern peatlands (approximately 16–30 Tg CH_4 yr^{-1}; Spahni *et al* 2011, Bruhwiler *et al* 2014). The coarse resolution ($0.5° \times 0.6°$) reanalysis meteorology used in the model simulations do not well represent sub-grid variability in soil wetness and temperature controls (von Fischer *et al* 2010, Sachs *et al* 2010, Sturtevant and Oechel 2013), which may lead to systematic biases when evaluating methane emissions at larger scales (Bohn and Lettenmaier 2010). However, we recognize that top-down

6

Table 1. Wetland methane (CH_4) emissions and associated surface inundation extent determined by regional modeling studies using satellite microwave based surface water (Fw) retrievals to define the spatial extent of methane producing area. The Fw inputs include those scaled using 15 day, monthly and annual Fw means and maximums, or a static multi-summer Fw mean climatology. The methane emissions determined in this study are reported for inundated and combined inundated/non-inundated wetland landscape fractions.

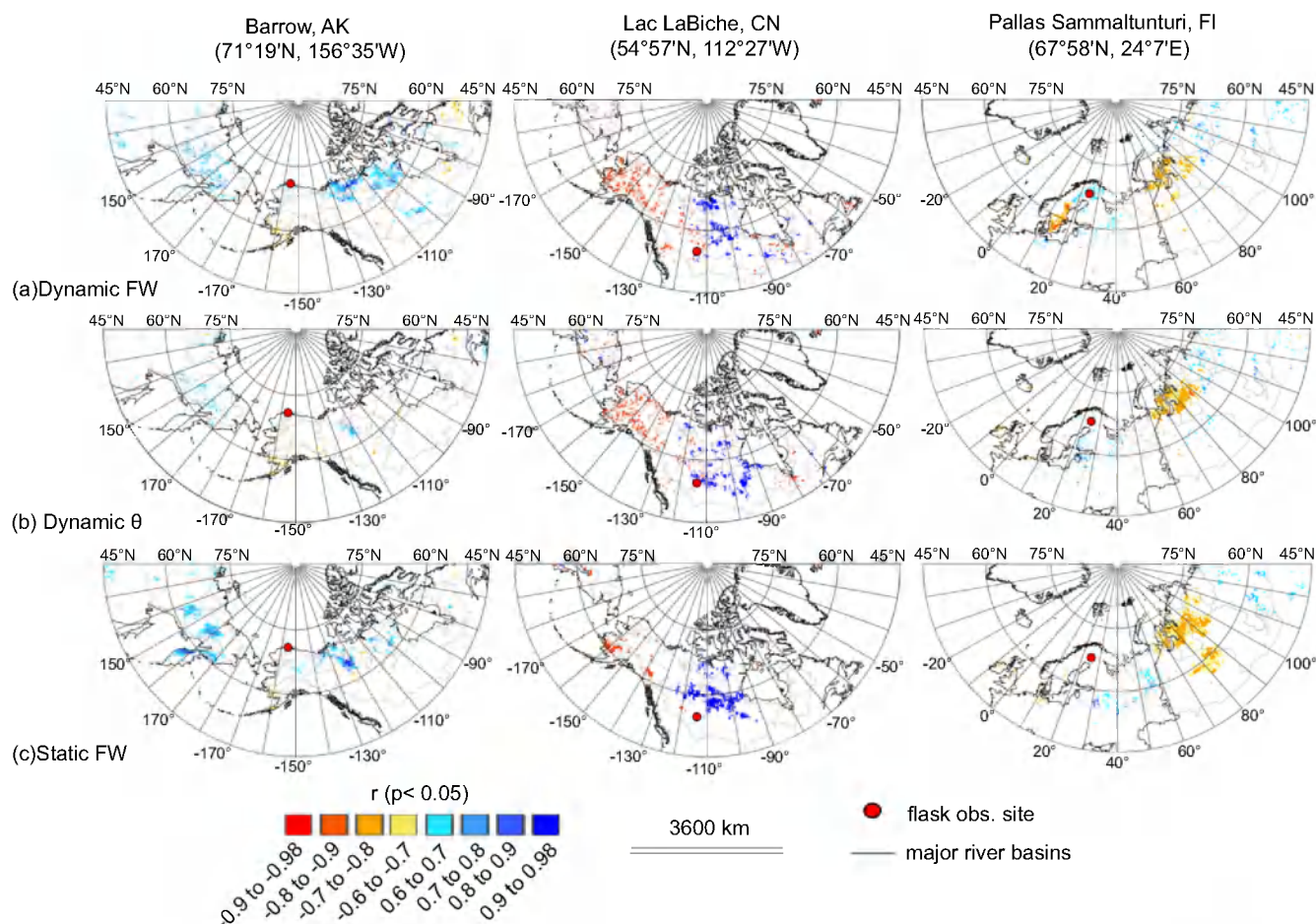| Study	Model	Domain	Fw source	Fw period	Fw scaling	Fw area (km^2)	Simulation period (CH_4)	Emissions ($Tg\ CH_4 yr^{-1}$) ± Std. Dev.
Petrescu et al (2010)	PEATLAND-VU	55°–70° N	Prigent et al (2007)	1993–2000	Monthly Clim. (avg.)	1.6×10^6	2001–2006	
					Adjusted area	4.4×10^6		89
Ringeval et al (2010)	ORCHIDEE	>50° N	Prigent et al (2007)	1993–2000	Month avg.	—	1993–2000	41
Riley et al (2011)	CLM4Me	45°–70° N	Prigent et al (2007)	1993–2000	Month avg.	2 to 3×10^6	1995–1999	70
Spahni et al (2011)	LPJ-WHyMe	45°–90° N	Prigent et al (2007)	1993–2000	Month avg.	2.1×10^6	2004	38.5–51.1
Wania et al (2013)	LPJ-WHyMe	>45° N	Prigent et al (2007), Papa et al (2010)	1993–2004	Annual clim. (avg.)	—	1993–2004	40
Wania et al (2013), Melton et al (2013)	LPJ-Bern	35°–90° N	Prigent et al (2007), Papa et al (2010)	1993–2004	Monthly clim. (avg.)	—	2004	81
This study (all areas)	JULES-TCF	45°–80° N	Jones et al (2010), Watts et al (2012)	2003–2011	15 day avg.	8.4×10^5	2003–2011	53.2 ± 1.9
This study (inundated only)	JULES-TCF	45°–80° N	Jones et al (2010), Watts et al (2012)	2003–2011	15 day avg.	—	2003–2011	5.4 ± 0.3
					15 day max.	1.1×10^6		7.5 ± 0.3
					Month avg.	8.9×10^5		5.5 ± 0.3
					Month max.	1.3×10^6		8.4 ± 0.3
					Annual avg.	9.7×10^5		5.8 ± 0.2
					Annual max.	1.6×10^6		10.8 ± 0.4
					Annual clim. (avg.)	1.5×10^6		5.9 ± 0.3

Figure 4. Regional Pearson correlation (r) between mean summer (May through September) dry air mole fractions (nmol CH_4 mol^{-1}) from NOAA ESRL flask sites in Alaska, Canada, and Finland, and modeled methane emissions (tonne CH_4 $cell^{-1}$) for sub-grid inundated (Fw) and non-inundated surface moisture (θ) conditions. Methane emissions from inundated surfaces reflect model simulations using dynamic 15 day Fw inputs, or static Fw climatology for the 2003–11 summer period. The correlation significance is determined at a minimum 95% probability level.

inversion analyses are also prone to uncertainties from atmospheric transport conditions and the limited number of observation sites within high latitude regions (Berchet *et al* 2013, Nisbet *et al* 2014).

In northern wetlands, 80–98% of annual methane emissions occur during the summer (Alm *et al* 1999, Jackowicz-Korczyński *et al* 2010, Song *et al* 2012) due to strong thermal controls on methane production, carbon substrate and water availability (Ström *et al* 2003, Christensen *et al* 2003, Wagner *et al* 2009). The influence of summer warming on regional methane emissions was apparent in the model simulations, with peak efflux occurring in June and July (figure S2). This seasonal pattern has been observed in atmospheric methane mixing ratios across the Arctic (Aalto *et al* 2007, Fisher *et al* 2011, Pickett-Heaps *et al* 2011). Also evident was the impact of wet/dry cycles on regional methane contributions, with annual summer emission budgets fluctuating by ±4%, relative to the 2003–11 mean. The modeled emissions were lowest in 2004 despite anomalously high temperatures throughout the boreal-Arctic region (Chapin *et al* 2005), due to drought conditions in Alaska and northern

Canada. In contrast, higher emissions in 2005 resulted from warm and wet weather in North America.

Surface moisture variability also influenced the correspondence between modeled emissions and summer atmosphere methane concentrations from the regional flask measurements. Regions showing a positive correspondence between modeled methane emissions and atmosphere concentrations largely reflected transport trajectories indicated in the HYSPLIT simulations (figure S3), with stronger agreement ($r > 0.7$, $p \leqslant 0.05$) occurring in areas characterized as open water or prone to periodic inundation (figure 4). Immediate to the flask sites, mean summer inundation varied from 2 to 10%, with moist soil fractions accounting for >85% of simulated emissions. At Lac LaBiche, annual emissions variability corresponding to wet soil fractions agreed well ($r = 0.96$, $p = 0.02$) with the flask observations. In contrast, relatively poor agreement was observed at Barrow and Sammaltunturi where emission patterns for inundated portions of the landscape corresponded more closely with atmospheric methane concentrations (table 2). At Barrow, the correspondence was similar ($r > 0.43$, $p \leqslant 0.12$) for model

simulations using dynamic 15 day or annual Fw inputs, reflecting methane source contributions from thermokarst lakes and inundated tundra in the surrounding landscape (Dlugokencky *et al* 1995). In contrast, the modeled emissions at Sammaltunturi corresponded closely ($r = 0.86$, $p < 0.01$) with flask observations when accounting for 15 day variability in Fw extent, but showed minimal agreement when using annual Fw inputs. This discrepancy may be attributed to less open water cover in the surrounding region and a tendency for summer precipitation events to produce intermittent flooding due to shallow soil layers and limited drainage (Aalto *et al* 2007). These results differ from the Lac LaBiche site, where nearby peatlands are characterized by deeper layers of surface litter and moss (Dlugokencky *et al* 2011) that can substantially reduce surface water coverage.

3.3. Fw temporal scaling effects on summer methane budgets

Wetland studies have increasingly used satellite microwave remote sensing to quantify the extent of methane emitting area, given the strong microwave sensitivity to surface moisture and relative insensitivity to solar illumination constraints and atmospheric signal attenuation. Regional inundation information has been incorporated into model simulations using monthly, annual, or static multi-year Fw means (Ringeval *et al* 2010, Petrescu *et al* 2010, Hodson *et al* 2011, Riley *et al* 2011, Spahni *et al* 2011, Meng *et al* 2012, Wania *et al* 2013). However, our simulation results show that temporal Fw scaling can lead to substantial differences in methane emission estimates (table 1).

In this analysis, inundation extent within the boreal-Arctic wetlands increased by 6–15% and 13–31% when using respective mean monthly or annual AMSR-E Fw inputs instead of finer (15 day) temporal intervals. The coarser Fw temporal inputs resulted in respective increases in estimated methane emission budgets by 6% ($t = 3.5$, $p < 0.01$) and 17% ($t = 8.7$, $p < 0.01$) in Eurasia, relative to simulations using finer 15 day Fw temporal inputs. The impacts of Fw temporal scaling in North America were not significant ($t \leqslant 0.7$, $p > 0.5$), with corresponding increases of 0.7% (Fw monthly) and 2% (Fw annual) in estimated annual methane emissions. The observed emissions sensitivity to Fw scaling in Eurasia primarily results from precipitation and flooding events in early summer, followed by mid-summer drying (Serreze and Etringer 2003). As a result, Fw means considered over longer time intervals in these regions may be biased towards spring inundation conditions, and may not reflect regional decreases in surface wetness occurring during the warmer mid-summer months. Directly incorporating Fw maximums, sometimes used to quantify multi-year surface hydrology trends (Bartsch *et al* 2012, Watts *et al* 2012), also led to substantial increases ($t > 9.66$, $p < 0.01$) in estimated methane emissions by 23–38% in North America and 21–54% in Eurasia for 15 day to annual time intervals relative to simulations using static Fw means.
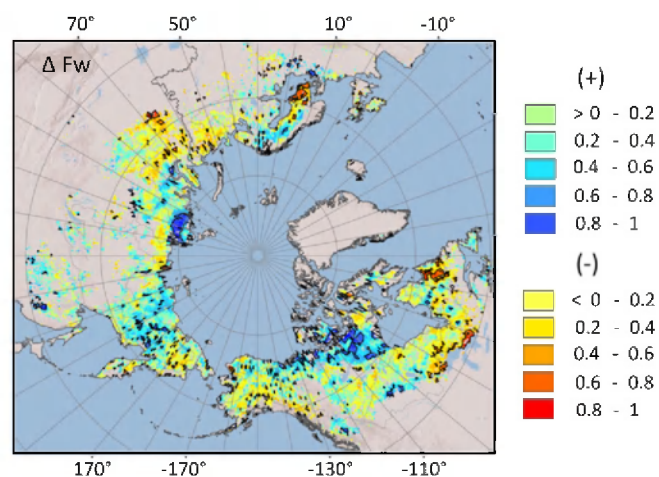

Figure 5. Recent summer AMSR-E Fw wetting and drying trends in the northern ($\geqslant 45°$ N) wetland regions, indicated by Mann-Kendall tau rank coefficients. Positive (negative) tau represents an increase (decrease) in surface water cover. Black polylines denote areas having significant ($p < 0.05$, $|tau| > 0.6$) change in surface water extent over the 2003–11 satellite observation record.

3.4. Potential impact of regional wetting and drying trends on methane emission budgets

Significant ($p < 0.05$) increases in surface inundation were observed over 4% (7.1×10^5 km^2) of the high latitude wetlands domain from 2003 to 2011, with substantial Fw wetting occurring within northern tundra and permafrost affected landscapes (figure 5). The extent of wetting increased to 6% (9.7×10^5 km^2) when including regions with slightly weaker trends ($p < 0.1$). While the regional wetting patterns may correspond with shifts in northward atmospheric moisture transport (Rawlins *et al* 2009, Skific *et al* 2009, Dorigo *et al* 2012, Screen 2013), trends within the Arctic Rim may be more closely influenced by thermokarst expansion, reductions in seasonal ice cover (Smith *et al* 2005, Rowland *et al* 2010, Watts *et al* 2012), and summer warming (figure 6(a)). In portions of western Siberia, localized cooling and residual winter snow melt (Cohen *et al* 2012) may also contribute to surface wetting. Regional drying was also observed across 3% (5.3×10^5 km^2, $p < 0.05$) and 5% (7.6×10^5 km^2, $p < 0.1$) of the northern wetland domain, particularly in northern boreal Alaska, eastern Canada and Siberia (figure 5). These declines in surface water extent may result from an increase in summer evaporative demand (Arp *et al* 2011) and the terrestrialization of open water environments following lake drainage (Payette *et al* 2004, Jones *et al* 2011b, Roach *et al* 2011, Helbig *et al* 2013).

The combined influence of warming and wetting in the AMSR-E Fw and reanalysis surface meteorology records contributed to an increase in methane emissions across 6% ($p < 0.05$, figure 6(b)) to 21% ($p < 0.1$) of the boreal-Arctic domain. This finding is similar to a projected 15% increase in methane emitting area with continued climate change in the northern wetland regions (Gao *et al* 2013). The corresponding mean rates of methane increase from 2003 to 2011 were 0.07

Table 2. Mean summer fractional water (Fw) inundation and Pearson correspondence (r, with associated significance) between flask station dry air mole fractions (nmol CH_4 mol^{-1}) and cumulative methane emission estimates (tonne CH_4 grid $cell^{-1}$) within a 3×3 window centered at Barrow (BRW), Lac LaBiche (LLB) and Pallas Sammaltunturi (PAL). The model simulations incorporate dynamic 15 day or mean annual Fw; non-inundated grid cell fractions are regulated by surface soil moisture content (θ).

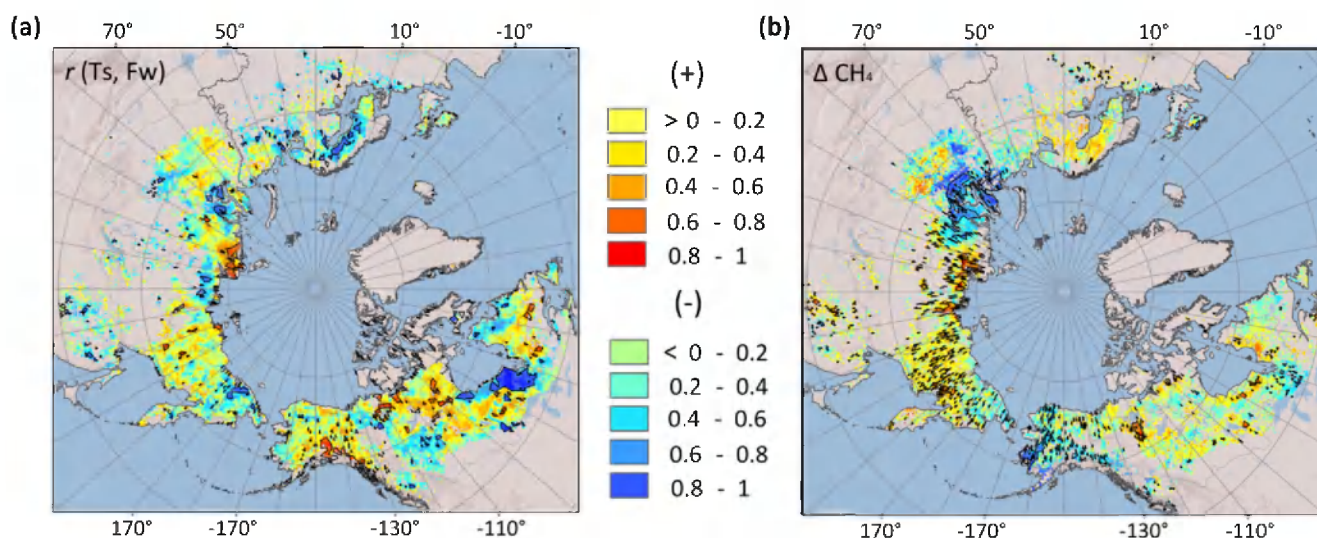| Location	Fw inundation (%)	Dynamic Fw	Annual Fw	θ	Fw + θ
			r		
BRW	5–15%	0.46 ($p = 0.11$)	0.43 ($p = 0.12$)	−0.14 ($p = 0.36$)	0.05 ($p = 0.45$)
LLB	3–4%	0.65 ($p = 0.24$)	0.74 ($p = 0.18$)	0.94 ($p = 0.03$)	0.96 ($p = 0.02$)
PAL	1–3%	0.86 ($p < 0.01$)	0.02 ($p = 0.48$)	0.10 ($p = 0.4$)	0.13 ($p = 0.37$)

Figure 6. Regional (a) Pearson correlations (r) between summer MERRA reanalysis surface soil temperature (T_s) and AMSR-E Fw inundation extent from 2003 to 2011, and (b) trends (Mann-Kendall tau) in wetland methane (CH_4) emissions for inundated and wet soil landscapes. Areas of significant ($p < 0.05$) correlation or trend are indicated by the black polylines.

and 0.11 ± 0.02 Tg CH_4 yr^{-1}, respectfully, and occurred primarily in Canada and eastern Siberia where summer warming has been observed in both *in situ* measurements and reanalysis records (figure S4, Screen, Simmonds (2010), Smith *et al* 2010, Walsh *et al* 2011). A decrease in modeled methane emissions, associated with surface drying and cooling patterns, was also observed across 7% ($p < 0.05$; -0.12 ± 0.03 Tg CH_4 yr^{-1}) and 15% ($p < 0.1$; $-0.15 \pm$ Tg CH_4 yr^{-1}) of the study area, and offset regional gains in the methane emissions. When including all regions showing significant change ($|t| > 3.6$; $p < 0.05$), as indicated by the linear regression analysis (without grid cell screening using the more conservative Mann-Kendall tau), the respective rates of increase and decrease in boreal-Arctic wetland emissions were 0.56 ± 0.16 Tg CH_4 yr^{-1} and -0.38 ± 0.07 Tg CH_4 yr^1.

4. Conclusions

Northern boreal-Arctic ecosystems may be especially vulnerable to methane emissions given climate warming, abundant soil carbon stocks, and a predominately wet landscape (Isaksen *et al* 2011, van Huissteden *et al* 2011, Olefeldt

et al 2013). We found that 5% of northern wetlands were characterized by open water or emergent vegetation, with the majority of inundation occurring in the Canadian Shield lowlands and Ob-Yenisei drainage basins. Areas of significant ($p < 0.05$) increase in surface water extent were more prevalent within the Arctic Rim and may coincide with heightened summer precipitation (Landerer *et al* 2010, Screen 2013) or high latitude permafrost thaw (Rowland *et al* 2010, Watts *et al* 2012). The combined effect of surface wetting and warming contributed to regional increases of 0.56 Tg CH_4 yr^{-1} in estimated methane emissions, relative to the 2003–11 mean. Our analysis also revealed surface drying throughout the boreal zones of southern Sweden, western Russia and eastern Canada, as has been anticipated with increasing summer temperatures and drought conditions in the sub-Arctic (Frolking *et al* 2006, Tarnocai 2006). This landscape drying contributed to a 0.38 Tg CH_4 yr^{-1} decrease in summer emissions, and largely offset any increases in region-wide methane release.

Regional modeling studies should consider the potential impacts of Fw scaling when prescribing the extent of methane emitting area in northern wetland regions, given the dynamic nature of surface water in northern landscapes (Schroeder

et al 2010, Bartsch *et al* 2012, Watts *et al* 2012). Our model sensitivity analysis shows significant differences in estimated annual emissions determined from coarse monthly or annual Fw relative to finer scale (15 day) inundation inputs. Although the estimated emissions rate of 53 Tg $CH_4 \, yr^{-1}$ is similar to the results from previous studies, it may over-estimate the magnitude of methane release from pan-boreal and Arctic wetland regions, given difficulties accounting for finer scale soil temperature and moisture heterogeneity (Sachs *et al* 2008, Parmentier *et al* 2011, Muster *et al* 2013) using coarse $\geqslant 0.5°$ reanalysis information. The NASA Soil Moisture Active Passive (SMAP) mission (Entekhabi *et al* 2010) is scheduled to launch in late-2014 and will provide new global satellite L-band active and passive microwave observations of the land surface, with regular monitoring of northern soil thermal and moisture dynamics at 1–2 day intervals and moderate (3–9 km) spatial scales. These new observations may provide for the improved quantification of regional patterns and temporal dynamics in surface environmental conditions, which is needed to reduce uncertainty in regional and global methane emissions.

Acknowledgements

References

Aalto T, Hatakka J and Lallo M 2007 Topospheric methane in northern Finland: seasonal variations, transport patterns and correlations with other trace gases *Tellus* B **59** 251–9

Alm J, Schulman L, Walden J, Nykänen H, Martiknainen P J and Silvola J 1999 Carbon balance of a boreal bog during a year with an exceptionally dry summer *Ecology* **80** 161–74

Arp C D, Jones B M, Urban F E and Grosse G 2011 Hydrogeomorphic processes of thermokarst lakes with grounded-ice and floating-ice regimes on the Arctic coastal plain, Alaska *Hydrol. Process* **25** 2422–38

Aselmann I and Crutzen P J 1989 Global distribution of natural freshwater wetlands and rice paddies, their net primary productivity, seasonality and possible methane emissions *J. Atmos. Chem.* **8** 307–58

Bartsch A, Trofaier A M, Hayman G, Sabel D, Schlaffer S, Clark D B and Blyth E 2012 Detection of open water dynamics with ENVISAT ASAR in support of land surface modeling at high latitudes *Biogeosciences* **9** 703–14

Berchet A *et al* 2013 Towards better error statistics for atmospheric inversions of methane surface fluxes *Atmos. Chem. Phys.* **13** 7115–32

Blodau C and Moore T R 2003 Micro-scale CO_2 and CH_4 dynamics in a peat soil during a water fluctuation and sulfate pulse *Soil Biol. Biogeochem.* **35** 535–47

Bloom A A, Palmer P I, Fraser A, Reay D S and Frankenberg C 2010 Large-scale controls of methanogenesis inferred from methane and gravity spaceborne data *Science* **327** 322–5

Bohn T J and Lettenmaier D P 2010 Systematic biases in large-scale estimates of wetland methane emissions arising from water table formulations *Geophys. Res. Lett.* **37** L22401

Bohn T J *et al* 2013 Modeling the large-scale effects of surface moisture heterogenieity on wetland carbon fluxes in the west Siberian lowland *Biogeosciences* **10** 6559–76

Brown J, Ferrians O J Jr, Heginbottom J A and Melnikov E S 1998 *Circum-Arctic Map of Permafrost and Ground-Ice Conditions* (Boulder, CO: National Snow and Ice Data Center/World Data Center for Glaciology) Digital Media

Bruhwiler L M, Dlugokencky E, Masarie K, Ishizawa M, Andrews A, Miller J, Sweeney C, Tans P and Worthy D 2014 CarbonTracker-CH_4: an assimilation system for estimating emissions of atmospheric methane *Atmos. Chem. Phys. Discuss.* **14** 2175–233

Chapin F S III *et al* 2005 Role of land-surface changes in Arctic summer warming *Science* **310** 657–60

Christensen T R, Ekberg A, Ström L, Mastepanov M, Panikov N, Öquist M, Svensson B H, Nykänen H, Martikainen P J and Oskarsson H 2003 Factors controlling large scale variations in methane emissions from wetlands *Geophys. Res. Lett.* **30** 1414

Clark D B *et al* 2011 The Joint UK land environmental simulator (JULES), model description-part 2: carbon fluxes and vegetation dynamics *Geosci. Model Dev.* **4** 701–22

Cohen J L, Furtado J C, Barlow M A, Alexeev V A and Cherry J E 2012 Arctic warming, increasing snow cover and widespread boreal winter cooling *Environ. Res. Lett.* **7** 014007

Desyatkin A R, Takakai F, Fedorov P P, Nikolaeva M C, Desyatkin R V and Hatano R 2009 CH_4 emission from different stages of thermokarst formation in central Yakutia, east Siberia *Soil Sci. Plant Nutri.* **55** 558–70

Ding Q and Wang B 2005 Circumglobal teleconnection in the northern hemisphere summer *J. Climate* **18** 3483–505

Dlugokencky E J, Steele L P, Lang P M and Masarie K A 1995 Atmospheric methane at Mauna Loa and Barrow observatories: presentation and analysis of in situ measurements *J. Geophys. Res.* **100** 103–13

Dlugokencky E J *et al* 2009 Observational constraints on recent increases in the atmospheric CH_4 burden *Geophys. Res. Lett.* **36** L18803

Dlugokencky E J, Nisbet E G, Fisher R and Lowry D 2011 Global atmospheric methane: budget, changes and dangers *Phil. Trans. R. Soc.* A **369** 2058–72

Dlugokencky E J, Lang P M, Crotwell A M, Masarie K A and Crotwell M J 2013 Atmospheric Methane Dry Air Mole Fractions from the NOAA ESRL Carbon Cycle Cooperative Global Air Sampling Network, 1983-2012, Version: 2013-08-28 ftp://aftp.cmdl.noaa.gov/data/trace_gases/ch4/flask/surface/

Dorigo W, de Jeu R, Chung D, Parinussa R, Liu Y, Wagner W and Fernández-Prieto D 2012 Evaluating global trends (1988–2010) in harmonized multi-satellite surface moisture *Geophys. Res. Lett.* **39** L18405

Draxler R R and Rolph G D 2013 HYSPLIT (HYbrid Single-Particle Lagrangian Integrated Trajectory) Model access via NOAA ARL READY Website. NOAA Air Resources Laboratory, College Park, MD http://www.arl.noaa.gov/HYSPLIT.php

Elberling B, Michelsen A, Schädel C, Schuur E A, Christiansen H H, Berg L, Tamstorf M P and Sigsgaard C 2013 Long-term CO_2 production following permafrost thaw *Nature Clim. Change* **3** 890–4

Entekhabi D *et al* 2010 The soil moisture active passive (SMAP) mission *Proc. IEEE* **98** 704–16

Fisher R E *et al* 2011 Arctic methane sources: isotopic evidence for atmospheric inputs *Geophys. Res. Lett.* **38** L21803

Franzén L G, Lindberg F, Viklander V and Walther A 2012 The potential peatland extent and carbon sink in Sweden, as related to the peatland/ice age hypothesis *Mires & Peat* **10** 1–19

Frolking S, Roulet N and Fuglestvedt J 2006 How northern peatlands influence the earth's radiative budget: sustained methane emission verses sustained carbon sequestration *J. Geophys. Res.* **111** G01008

Gao X, Schlosser C A, Sokolov A, Anthony K W, Zhuang Q and Kicklighter D 2013 Permafrost degradation and methane: low risk of biogeochemical climate-warming feedback *Environ. Res. Lett.* **8** 035014

Gedney N, Cox P M and Huntingford C 2004 Climate feedback from wetland emissions *Geophys. Res. Lett.* **31** L20503

Glagolev M, Kleptsova I, Filippov I, Maksyutov S and Machida T 2011 Regional methane emission from west Siberia mire landscapes *Environ. Res. Lett.* **6** 045214

Gunnarsson U and Löfroth M 2009 *Wetlands Inventory—Results from 25 Years of Inventory. National Final Report for Wetland Inventory (VMI) in Sweden). Naturvårdsverket Rapport* **5925** 120

Harden J W *et al* 2012 Field information links permafrost carbon to physical vulnerabilities of thawing *Geophys. Res. Lett.* **39** L15704

Helbig M, Boike J, Langer M, Schreiber P, Runkle B R K and Kutzbach L 2013 Spatial and seasonal variability of polygonal tundra water balance: lena river delta, northern Siberia (Russia) *Hydrogeol. J.* **21** 133–47

Hodson E L, Poulter B, Zimmermann N E, Prigent C and Kaplan J O 2011 The El niño southern oscillation and wetland methane interannual variability *Geophys. Res. Lett.* **38** L08810

Hugelius G, Tarnocai C, Broll G, Canadell J G, Kuhry P and Swanson D K 2013 The northern circumpolar soil carbon database: spatially distributed datasets of soil coverage and soil carbon storage in the northern permafrost regions *Earth Syst. Sci. Data* **5** 3–13

Isaksen I S A, Gauss M, Myhre G, Walter Anthony K M and Ruppel C 2011 Strong atmospheric chemistry feedback to climate warming from Arctic methane emissions *Glob. Biochem. Cy.* **25** GB2002

Jackowicz-Korczyński M, Christensen T R, Bäckstrand K, Crill P, Friborg T, Mastepanov M and Ström L 2010 Annual cycle of methane emission from a subarctic peatland *J. Geophys. Res.* **115** G02009

Joabsson A, Christensen T R and Wallén B 1999 Vascular plant controls on methane emissions from northern peatforming wetlands *Trends Ecol. Evol.* **14** 385–8

Jones B M, Grosse G, Arp C D, Jones M C, Walter Anthony K M and Romanovsky V E 2011b Modern thermokarst lake dynamics in the continuous permafrost zone, northern seward peninsula, Alaska *J. Geophys. Res.* **116** G00M03

Jones L A, Ferguson C R, Kimball J S, Zhang K, Chan S T K, McDonald K C, Njoku E G and Wood E F 2010 Satellite microwave remote sensing of daily land surface air temperature minima and maxima from AMSR-E *IEEE J. Sel. Top. Appl. Earth Obs. Remote Sens.* **3** 111–23

Jones L A and Kimball J S 2011a Daily global land surface parameters derived from AMSR-E (Boulder, CO: National Snow and Ice Data Center) Digital media. nsidc.org/data/nsidc-0451.html

Jones M O, Kimball J S and Jones L A 2013 Satellite microwave detection of boreal forest recovery from the extreme 2004 wildfires in Alaska and Canada *Glob. Change Biol.* **19** 3111–22

Kao-Kniffin J, Freyre D S and Balser T C 2010 Methane dynamics across wetland plant species *Aq. Bot.* **93** 107–13

Kim Y, Kimball J S, Glassy J and McDonald K C 2013 Measures Global Record of Daily Landscape Freeze/Thaw Status.

Version 2 (Boulder, CO: NASA DAAC at the National Snow and Ice Data Center) http://nsidc.org/data/nsidc-0477

Kimball J S, Jones L A, Zhang K, Heinsch F A, McDonald K C and Oechel W C 2009 A satellite approach to estimate land-atmosphere CO_2 exchange for boreal and Arctic biomes using MODIS and AMSR-E *IEEE Geosci. Remote Sens.* **47** 569–87

Koven C D, Ringeval B, Friedlingstein P, Ciais P, Cadule P, Khvorostyanov D, Krinner G and Tarnocai C 2011 Permafrost carbon-climate feedbacks accelerate global warming *Proc. Natl. Acad. Sci.* **108** 14769–74

Landerer F D, Dickey J O and Güntner A 2010 Terrestrial water budget of the Eurasian pan-from GRACE satellite measurements during 2003–2009 *Geophys. Res. Atmos.* **115** D23115

Laurion I, Vincent W F, MacIntyre S, Retamal L, Dupont C, Francus P and Pienitz R 2010 Variability in greenhouse gas emissions from permafrost thaw ponds *Limnol. Oceanogr.* **55** 115–33

Lehner B and Döll P 2004 Development and validation of a global database of lakes, reservoirs and wetlands *J. Hydrol.* **296** 1–22

Lelieveld J, Crutzen P J and Dentener F J 1998 Changing concentration, lifetime and climate forcing of atmospheric methane *Tellus* B **50** 128–50

Long K D, Flanagan L B and Cai T 2010 Diurnal and seasonal variation in methane emissions in a northern canadian peatland measured by eddy covariance *Glob. Change Biol.* **16** 2420–35

Lupascu M, Wadham J L, Hornibrook E R C and Pancost R D 2012 Temperature sensitivity of methane production in the permafrost active layer at Stordalen, Sweden: a comparison with non-permafrost northern wetlands *Arct. Antarct. Alp. Res.* **44** 469–82

Matthews E and Fung I 1987 Methane emissions from natural wetlands: global distribution, area, and environmental characteristics of sources *Glob. Biogeochem. Cycle* **1** 61–86

McGuire A D *et al* 2012 An assessment of the carbon balance of Arctic tundra: comparisons among observations, process models, and atmospheric inversions *Biogeosciences* **9** 3185–204

Melton J R *et al* 2013 Present state of global wetland extent and wetland methane modeling: conclusions from a model intercomparison project (WETCHIMP) *Biogeosciences* **10** 753–88

Meng L, Hess P G M, Mahowald N M, Yavitt J B, Riley W J, Subin Z M, Lawrence D M, Swenson S C, Jauhiainen J and Fuka D R 2012 Sensitivity of wetland methane emissions to model assumptions: application and model testing against site observations *Biogeosciences* **9** 2793–819

Muster S, Heim B, Abnizova A and Boike J 2013 Water body distributions across scales: a remote sensing based comparison of three Arctic tundra wetlands *Remote Sens.* **5** 1498–523

Nisbet E G, Dlugokencky E J and Bousquet P 2014 Methane on the rise—again *Science* **31** 493–5

Olefeldt D, Turetsky M R, Crill P M and McGuire A D 2013 Environmental and physical controls on northern terrestrial methane emissions across permafrost zones *Glob. Change Biol.* **19** 589–603

Parmentier F J W, van Huissteden J, van der Molen M K, Schaepman-Strub G, Karsanaev S A, Maximov T C and Dolman A J 2011 Spatial and temporal dynamics in eddy covariance observations of methane fluxes at a tundra site in northeastern Siberia *J. Geophys. Res.* **116** G03016

Papa F, Prigent C, Aires F, Jimenez C, Rossow W B and Matthews E 2010 Interannual variability of surface water extent at global scale 1993–2004 *J. Geophys. Res. Atmos.* **115** D12111

Payette S, Delwaide A, Caccianiga M and Beauchemin M 2004 Accelerated thawing of subarctic peatland permafrost over the last 50 years *Geophys. Res. Lett.* **31** L18208

Petrescu A M R, van Beek L P H, van Huissteden J, Prigent C, Sachs T, Corradi C A R, Parmentier F J W and Dolman A J 2010 Modeling regional to global CH4 emissions of boreal and arctic wetlands *Glob. Biogeochem. Cycle* **24** GB4009

Pickett-Heaps C A, Jacob D J, Wecht K J, Kort E A, Wofsy S C, Diskin G S, Worthy D E J, Kaplan J O, Bey I and Drevet J 2011 Magnitude and seasonality of wetland methane emissions from the hudson bay lowlands (Canada) *Atmos. Chem. Phys.* **11** 3773–9

Prigent C, Papa F, Aires F, Rossow W B and Matthews E 2007 Global inundation dynamics inferred from multiple satellite observations 1993–2000 *J. Geophys. Res. Atmos.* **112** D12107

Rawlins M A, Ye H, Yang D, Shiklomanov A and McDonald K C 2009 Divergence in seasonal hydrology across northern Eurasia: emerging trends and water cycle linkages *J. Geophys. Res. Atmos.* **114** D18119

Reeburgh W S, King J Y, Regli S K, Kling G W, Auerbach N A and Walker D A 1998 A CH_4 emission estimate for the Kuparuk river basin, Alaska *J. Geophys. Res. Atmos* **103** 29005–13

Reichle R H, Koster R D, De Lannoy G J M, Forman B A, Liu Q, Mahanama S P P and Toure A 2011 Assessment and enhancement of MERRA land surface hydrology estimates *J. Clim.* **24** 6322–38

Riley W J, Subin Z M, Lawrence D M, Swenson S C, Torn M S, Meng L, Mahowald N M and Hess P 2011 Barriers to predicting changes in global terrestrial methane fluxes: analyses using CLM4Me, a methane biogeochemistry model integrated in CESM *Biogeosciences* **8** 1925–53

Rinne J, Riutta T, Pihlatie M, Aurela M, Haapanala S, Tuovinen J-P and Tuittila E-S 2007 Annual cycles of methane emission from a boreal fen measured by the eddy covariance technique *Tellus* B **59** 449–57

Ringeval B, de Noblet-Ducoudré N, Ciais P, Bousquet P, Prigent C, Papa F and Rossow W B 2010 An attempt to quantify the impact of changes in wetland extent on methane emissions on the seasonal and interannual time scales *Glob. Biogeochem. Cycle* **24** GB2003

Rinsland C P, Dufour G, Boone C D, Bernath P F, Chiou L, Coheur P-F, Turquety S and Clerbaux C 2007 Satellite boreal measurements over Alaska and Canada during June–July 2004: simultaneous measurements of upper tropospheric CO, C_2H_6, HCN, CH_3Cl, CH_4, C_2H_2, CH_3OH, HCOOH, OCS and SF_6 mixing ratios *Glob. Biogeochem. Cycle* **21** GB3008

Roach J, Griffith B, Verbyla D and Jones J 2011 Mechanisms influencing changes in lake area in Alaskan boreal forest *Glob. Change Biol.* **17** 2567–83

Rodell M *et al* 2004 The global land data assimilation system *Bull. Am. Meteorol. Soc.* **85** 381–94

Rolph G D 2013 Real-time Environmental Applications and Display sYstem (READY) Website. NOAA Air Resources Laboratory, College Park, MD http://www.ready.noaa.gov

Rover J, Ji L, Wylie B K W and Tieszen L L 2012 Establishing water body areal extent trends in interior Alaska from multitemporal landsat data *Remote Sens. Lett.* **3** 595–604

Rowland J C *et al* 2010 Arctic landscapes in transition: responses to thawing permafrost *EOS Trans. Am. Geophys. Union* **91** 229–30

Sabrekov A F, Glagolev M V, Filippov I V, Kazantsev V S, Lapshina E D, Machida T and Maksyutov S S 2012 Methane emissions from north and middle taiga mires of western Siberia: Bc8 standard model *Moscow Soil Sci. Bull.* **67** 45–53

Sachs T, Wille C, Boike J and Kutzbach L 2008 Environmental controls on ecosystem-scale CH_4 emission from polygonal tundra in the Lena River Delta, Siberia *J. Geophys. Res.* **113** G00A03

Sachs T, Giebels M, Boike J and Kutzbach L 2010 Environmental controls on CH_4 emission from polygonal tundra on the microsite scale in the Lena River Delta, Siberia *Global Change Biol.* **11** 3096–110

Schneider J, Grosse G and Wagner D 2009 Land cover classification of tundra environments in the arctic lena delta based on landsat 7 ETM+ data and its application for upscaling of methane emissions *Remote Sens. Environ.* **113** 380–91

Schneider von Deimling T, Meinshausen M, Levermann A, Huber V, Frieler K, Lawrence D M and Brovkin V 2012 Estimating the near-surface permafrost-carbon feedback on global warming *Biogeosciences* **9** 649–65

Schroeder R, Rawlins M A, McDonald K C, Podest E, Zimmerman R and Kueppers M 2010 Satellite microwave remote sensing of north eurasian inundation dynamics: development of coarse-resolution products and comparison with high-resolution synthetic aperture radar data *Environ. Res. Lett.* **5** 015003

Screen J A and Simmonds I 2010 The central role of diminishing sea ice in recent Arctic temperature amplification *Nature* **464** 1334–7

Screen J A 2013 Influence of Arctic sea ice on European summer precipitation *Environ. Res. Lett.* **8** 044015

Serreze M C and Etringer A J 2003 Precipitation characteristics of the eurasian arctic drainage system *Int. J. Climatol.* **23** 1267–91

Skific N, Francis J A and Cassano J J 2009 Attribution of projected changes in atmospheric moisture transport in the Arctic: a self-organizing map perspective *J. Clim.* **22** 4135–53

Smith L C, Sheng Y, MacDonald G and Hinzman L D 2005 Disappearing arctic lakes *Science* **308** 1429

Smith S L, Romanovsky V E, Lewkowicz A G, Burn C R, Allard M, Clow G D, Yoshikawa K and Throop J 2010 Thermal state of permafrost in North America: a contribution to the international polar year *Permafr. Periglac. Process* **21** 117–35

Song C, Xu X, Sun X, Tian H, Sun L, Miao Y, Wang X and Guo Y 2012 Large methane emission upon spring thaw from natural wetlands in the northern permafrost region *Environ. Res. Lett.* **7** 034009

Spahni R *et al* 2011 Constraining global methane emissions and uptake by ecosystems *Biogeosciences* **8** 1643–65

Ström L, Ekberg A, Mastepanov M and Christensen T R 2003 The effect of vascular plants on carbon turnover and methane emissions from a tundra wetland *Glob. Change Biol.* **9** 1185–92

Sturtevant C S and Oechel W C 2013 Spatial variation in landscape-level CO_2 and CH_4 fluxes from arctic coastal tundra: influence from vegetation, wetness, and the thaw lake cycle *Glob. Change Biol.* **19** 2853–66

Tarnocai C 2006 The effect of climate change on carbon in Canadian peatlands *Glob. Planet. Change* **53** 222–32

Turetsky M R, Wieder R K, Vitt D H, Evans R J and Scott K D 2007 The disappearance of relict permafrost in boreal north America: effects on peatland carbon storage and fluxes *Glob. Change Biol.* **13** 1922–34

Turetsky M R, Treat C C, Waldrop M P, Waddington J M, Harden J W and McGuire A D 2008 Short-term response of methane fluxes and methanogen activity to water table and soil warming manipulations in an alaskan peatland *J. Geophys. Res. Biogeosci.* **113** G00A10

Turetsky M R *et al* 2014 A synthesis of methane emissions from 71 northern, temperate, and subtropical wetlands *Glob. Change Biol.* doi:10.1111/gcb.12580

van Huissteden J, Berrittella C, Parmentier F J W, Mi Y, Maximov T C and Dolman A J 2011 Methane emissions from permafrost thaw lakes limited by lake drainage *Nat. Clim. Change* **2** 119–23

von Fischer J C, Rhew R C, Ames G M, Fosdick B K and von Fischer P E 2010 Vegetation height and other controls of spatial variability in methane emissions from the Arctic coastal tundra at Barrow, Alaska *J. Geophys. Res.* **115** G00I03

Wagner D, Kobabe S and Liebner S 2009 Bacterial community structure and carbon turnover in permafrost-affected soils of the lena delta, northeastern Siberia *Can. J. Microbiol.* **55** 73–83

Waldrop M P, Wickland K P, White R III, Berhe A A, Harden J W and Romanovsky V E 2010 Molecular investigations into a globally important carbon pool: permafrost-protected carbon in alaskan soils *Glob. Change Biol.* **16** 2543–54

Walsh J E, Overland J E, Groisman P Y and Rudolf B 2011 Ongoing climate change in the Arctic *Ambio* **40** 6–16

Walter K M, Zimov S A, Chanton J P, Verbyla D and Chapin F S III 2006 Methane bubbling from siberian thaw lakes as a positive feedback to climate warming *Nature* **443** 71–5

Wania R *et al* 2013 Present state of global wetland extent and wetland methane modeling: methodology of a model inter-comparison project (WETCHIMP) *Geosci. Model Dev.* **6** 617–41

Watts J D, Kimball J S, Jones L J, Schroeder R and McDonald K C 2012 Satellite microwave remote sensing of contrasting surface water inundation changes within the Arctic-boreal region *Remote Sens. Environ.* **127** 223–36

Watts J D, Kimball J S, Parmentier F J W, Sachs T, Zona D, Oechel W, Tagesson T, Jackowicz-Korczyński M and Aurela M 2014 A satellite data driven biophysical modeling approach for estimating northern peatland and tundra CO_2 and CH_4 fluxes *Biogeosciences* **11** 1961–80

Wik M, Crill P M, Varner R K and Bastviken D 2013 Multiyear measurements of ebullitive methane flux from three subarctic lakes *J. Geophys. Res.* **118** 1307–21

Wille C, Kutzbach L, Sachs T, Wagner D and Pfeiffer E-M 2008 Methane emission from siberian arctic polygonal tundra: eddy covariance measurements and modeling *Glob.Change Biol.* **14** 1395–408

Yi Y, Kimball J S, Jones L A, Reichle R H and McDonald K C 2011 Evaluation of MERRA land surface estimates in preparation for the soil moisture active passive mission *J. Clim.* **24** 3797–816

Yi Y, Kimball J S, Jones L A, Reichle R H, Nemani R and Margolis H A 2013 Recent climate and fire disturbance impacts on boreal and arctic ecosystem productivity estimated using a satellite-based terrestrial carbon flux model *J. Geophys. Res.* **118** 1–17

Yu Z, Loisel J, Brosseau D P, Beilman D W and Hunt S J 2010 Global peatland dynamics since the last glacial maximum *Geophys. Res. Lett.* **37** L13402

Yue S, Pilon P, Phinney B and Cavadias G 2002 The influence of autocorrelation on the ability to detect trend in hydrological series *Hydrol. Process* **16** 1807–29

Zhang K, Kimball J S, Hogg E H, Zhao M, Oechel W C, Cassano J J and Running S W 2008 Satellite-based model detection of recent climate-driven changes in northern high-latitude vegetation productivity *J. Geophys. Res.* **113** G03033

Zhang X, He J, Zhang J, Polyakov I, Gerdes R, Inoue J and Wu P 2013 Enhanced poleward moisture transport and amplified northern high-latitude wetting trend *Nature Clim. Change* **3** 47–51

Zimov S A, Voropaev Y V, Semiletov I P, Davidov S P, Prosiannikov S F, Chapin F S III, Chapin M C, Trumbore S and Tyler S 1997 North Siberian lakes: a methane source fueled by pleistocene carbon *Science* **277** 800–1

Zhu X, Zhuang Q, Chen M, Sirin A, Melillo J, Kicklighter D, Sokolov A and Song L 2011 Rising methane emissions in response to climate change in northern eurasia during the 21st century *Environ. Res. Lett.* **6** 045211

Zhu X, Zhuang Q, Qin Z, Glagolev M and Song L 2013 Estimating wetland methane emissions from the northern high latitudes from 1990 to 2009 using artificial neural networks *Glob. Biochem. Cy.* **27** 592–604

Zona D, Oechel W C, Kochendorfer J, Paw U K T, Salyuk A N, Olivas P C, Oberbauer S F and Lipson D A 2009 Methane fluxes during the initiation of a large-scale water table manipulation experiment in the alaskan Arctic *Glob. Biogeochem. Cycle* **23** GB2013